Water Resources Research

RESEARCH ARTICLE
10.1029/2021WR031807

Retention Site Contribution Toward Silver Particle Immobilization in Porous Media

Janis E. Patiño[1], Francisco J. Pérez-Reche[2], and Verónica L. Morales[1]

[1]University of California, Davis, CA, USA, [2]University of Aberdeen, Aberdeen, UK

Key Points:

- Colloid retention assessment at six candidate retention sites showed depth invariant trends for variable saturation, velocity, and chemistry
- At the pore-scale the solid-water interface contributes the most to colloid retention, but only accounts for 0.5 of deposited mass
- xDLVO profiles at the interface-scale are in excellent agreement with pore-scale and Darcy-scale trends

Supporting Information:

Supporting Information may be found in the online version of this article.

Correspondence to:

V. L. Morales,
vermorales@ucdavis.edu

Citation:

Patiño, J. E., Pérez-Reche, F. J., & Morales, V. L. (2022). Retention site contribution toward silver particle immobilization in porous media. *Water Resources Research*, *58*, e2021WR031807. https://doi.org/10.1029/2021WR031807

Received 11 DEC 2021
Accepted 18 APR 2022

Author Contributions:

Conceptualization: Verónica L. Morales
Data curation: Janis E. Patiño
Formal analysis: Janis E. Patiño, Francisco J. Pérez-Reche, Verónica L. Morales
Funding acquisition: Verónica L. Morales
Investigation: Janis E. Patiño
Methodology: Janis E. Patiño, Francisco J. Pérez-Reche
Resources: Verónica L. Morales
Supervision: Francisco J. Pérez-Reche, Verónica L. Morales
Writing – original draft: Janis E. Patiño
Writing – review & editing: Francisco J. Pérez-Reche, Verónica L. Morales

Abstract This work investigates the role that pore structure plays in colloid retention across scales with a novel methodology based on image analysis. Experiments were designed to quantify–with robust statistics–the contribution from commonly proposed retention sites toward colloid immobilization. Specific retention sites include solid-water interface, air-water interface, air-water-solid triple point, grain-to-grain contacts, and thin films. Variable conditions for pore-water content, velocity, and chemistry were tested in a model glass bead porous medium with silver microspheres. Concentration signals from effluent breakthrough and spatial profiles of retained particles from micro X-ray Computed Tomography were used to compute mass balances and enumerate pore-scale regions of interest in three dimensions. At the Darcy-scale, retained colloids follow non-monotonic deposition profiles, which implicates effects from flow-stagnation zones. The spatial distribution of immobilized colloids along the porous medium depth was analyzed by retention site, revealing depth-independent partitioning of colloids. At the pore-scale, dominance and overall saturation of all retention sites considered indicated that the solid-water interface and wedge-shaped regions associated with flow-stagnation (grain-to-grain contacts in saturated and air-water-solid triple points in unsaturated conditions) are the greatest contributors toward retention under the tested conditions. At the interface-scale, xDLVO energy profiles were in agreement with pore-scale observations. Our calculations suggest favorable interactions for colloids and solid-water interfaces and for weak flocculation (e.g., at flow-stagnation zones), but unfavorable interactions between colloids and air-water interfaces. Overall, we demonstrate that pore-structure plays a critical role in colloid immobilization and that Darcy-, pore- and interface-scales are consistent when the pore structure is taken into account.

1. Introduction

The expanding use of engineered colloids in the manufacturing of medical and electrical appliances, textiles, paint protecting coverings, and consumer products has led to the accumulation of undesirable amounts of nano- and micro-size particles in the environment (Benn & Westerhoff, 2008; Goswami et al., 2017; Gottschalk et al., 2013; Keller et al., 2014). Of particular interest are silver particles, employed in the fabrication of detergents and anti-odor clothing because of their biocidal properties (Gottschalk et al., 2013; Maillard & Hartemann, 2013; Sondi & Salopek-Sondi, 2004; Zhang et al., 2016). Studies up to date have demonstrated that a large proportion of colloidal silver can enter sewers and the wastewater treatment train via erosion during silver-impregnated textile washing (Benn & Westerhoff, 2008; Keller et al., 2014). Furthermore, silver particle surfaces likely acquire a coating of surfactants (El Badawy et al., 2011; Geranio et al., 2009; Hedberg et al., 2012) and dissolved organic matter (Kaegi et al., 2011; Phenrat et al., 2008) along the sewer pathway, which increases the stability and persistence of the suspension. This raises concerns regarding the detrimental environmental and public health impact that stabilized antimicrobial silver-laden effluent and sludge may have on soil and aquatic systems where they are discharged (Benn et al., 2010; Benn & Westerhoff, 2008; Dimkpa et al., 2011; Gajjar et al., 2009; Kaegi et al., 2011; Keller et al., 2014; Mijnendonckx et al., 2013; Patiño et al., 2020). Regarding environmental health concerns, studies on soil microbial toxicity observed adverse effects on microbial growth, functions and diversity in soils, which became more pronounced over time (Samarajeewa et al., 2017; Sillen et al., 2015; Zhang et al., 2020). Regarding public health concerns, reports on the oral toxicity of silver colloids suggest that mammals may experience dose-dependent altered neurotransmitter levels and immunological effects (Hadrup & Lam, 2014; Park et al., 2010), and that the toxicity of silver particles increases with decreasing size (Kuempel et al., 2021). A sound understanding of the underlying physics that govern spreading and retention of micro and nano-particles in porous media is necessary to improve the accuracy of mechanistic models that describe their

transport. Such models are crucial for anticipating and ultimately preventing soil and groundwater contamination by engineered materials.

Macroscopic transport and retention of colloids is measured as deposited mass along the porous medium depth (depth profiles, DP) and/or concentration signals in the effluent (breakthrough curves, BT). Traditionally, these signals are described with mathematical models based on Colloid Filtration Theory (CFT). A classical view predicts exponentially decreasing DP from clean bead and first-order deposition kinetics assumptions (Yao et al., 1971). Deviations from CFT have been frequently observed in the presence of repulsive interactions between particles and collectors (unfavorable conditions); particularly resulting in the underestimation of the mass of immobilized particles (Bradford, Simunek, et al., 2006; Tufenkji & Elimelech, 2004). Particle retention under unfavorable conditions has been ascribed to deposition in secondary energy minimum (Shen et al., 2007), surface roughness (Morales et al., 2009; Rasmuson et al., 2017), concurrent favorable and unfavorable interactions between colloids and the porous media surface (Tufenkji & Elimelech, 2004), and surface charge heterogeneity (Cortis et al., 2006; Elimelech & O'Melia, 1990; Johnson et al., 1996). Anomalous DP behavior is common and is often associated with unique pore-scale retention mechanisms (Goldberg et al., 2014). Hyper-exponential DP have been explained by colloid straining in narrow pore spaces in addition to attachment to the soil-water interface (Bradford & Bettahar, 2005; Tosco et al., 2014). Uniform DP are thought to be controlled by blocking phenomena, where deposited particles prevent further colloid deposition (Adamczyk et al., 1994; Ko & Elimelech, 2000). Non-monotonic DP are associated to colloid accumulation at low-flow regions (Li et al., 2006a, 2006b) and to size-dependent deposition of polydisperse suspensions (Malgaresi et al., 2019). Monotonically increasing DP have been attributed to colloid-induced charge redistribution on the collectors (Chen et al., 2011). While variations to traditional CFT-based models have been successfully implemented to capture a subset of non-exponential DP behaviors (Tufenkji & Elimelech, 2005; Johnson et al., 2018), as of yet, information on the pore structure (including locations where multiple interfaces meet) is not yet implemented in such modeling approaches. Thus, sound evidence is lacking to confidently pair the pore-scale mechanisms represented in the models with the DP behavior they produce. High resolution X-ray computed tomography (XCT) has recently gained traction to address aspects of this knowledge gap (Leuther et al., 2020; Li et al., 2006a; Perez et al., 2020).

Microscopic variations in colloid retention occur largely as a result of the pore space geometry and its established flow field (Bradford & Torkzaban, 2008; Torkzaban et al., 2008). CFT employs a first approximation of the mass transfer rate between suspended and arrested particles by upscaling an assumed perfect sink at the solid-water (SW) interface (Yao et al., 1971). Nevertheless, the forces and torques that act on colloids near contact points where multiple interfaces meet are fundamentally different from those acting on a single interface (Bergendahl & Grasso, 1998; Gao et al., 2008; Torkzaban et al., 2007). Experimental observations (by various microscopic techniques) of colloid transport and deposition at the pore-scale have provided valuable insight on particle retention in locations other than the SW. Notable examples include: straining in too narrow pores (Bradford & Bettahar, 2005; Bradford et al., 2007; Bradford & Torkzaban, 2008; Tosco et al., 2014), accumulation in flow stagnant grain-to-grain contacts (GG) (Li et al., 2006a; Johnson et al., 2007, 2010; Lin et al., 2021), attachment to the air-water (AW) interface (Lazouskaya et al., 2006; Sirivithayapakorn & Keller, 2003; Wan & Wilson, 1994), pinning at the air-water-solid triple point (AWS; Chen & Flury, 2005; Crist et al., 2004; Morales et al., 2009; Rahmatpour et al., 2018; Wan & Tokunaga, 2005; Zevi et al., 2012), and straining in thin films of water (TF) adjacent to solid surfaces (Wan & Tokunaga, 1997). While this evidence highlights the relevance of pore space structure, it is not possible to determine the contributing weight of alternative retention sites from observations in a handful of pores located at the boundary of the transport experiment device. Assessing the significance of various contending pore-scale processes warrants statistical analysis from observations in numerous pores *within* the porous medium.

Nanoscopic interactions between colloids and the individual surfaces present in porous media are traditionally modeled by Derjaguin-Landau-Verwey-Overbeek (DLVO) theory. In principle, these surface interactions control the attachment efficiency–and consequently the deposition rate–in CFT models. Yet, a formal relationship between the two has not been established (Morales, Sang, et al., 2011; Phenrat et al., 2008). In DLVO theory, the total energy of interaction is given by the sum of van der Waals attraction (VDW) and electric double layer repulsion (EDL; Derjaguin, 1941; Verwey & Willem, 1947). Extended versions of DLVO (xDLVO) include additional interactions affected by complexity of the solution chemistry and presence of air bubbles (Birdi, 2008; Molnar, Johnson, et al., 2015). Furthermore, the occurrence of chemical heterogeneities and roughness on any of the approaching surfaces can significantly modify their interfacial interactions (Johnson et al., 2010; Torkzaban

& Bradford, 2016; Tufenkji & Elimelech, 2005). Relevant xDLVO interactions to this work include: charge screening from changes in ionic strength, which affect the EDL (Mills et al., 1994; Molnar, Johnson, et al., 2015; Polemio et al., 1980); steric interactions (ST) from surface adsorption of naturally occurring dissolved organic matter (Babakhani et al., 2017; Chen & Elimelech, 2006; Leuther et al., 2020; Molnar, Gerhard, et al., 2015; Morales, Sang, et al., 2011; Morales, Zhang, et al., 2011; Patiño et al., 2020; Phenrat et al., 2008); polar or Lewis acid-base interactions (AB) from the electron-acceptor and electron-donor nature of the two approaching materials (Van Oss, 2006); and hydrophobic interactions (HYD) between the particles and air bubbles under unsaturated conditions (Birdi, 2008; Crist et al., 2005; Kohli & Mittal, 2015). While substantial progress has been made to account for the pertinent colloidal interactions in typical groundwater systems, relating these surface energetics to pore-scale and Darcy-scale observations is not straight forward. This is mainly because during the process of deposition, particles interact with multiple planes simultaneously rather than the single infinite flat plane modeled in the theory. To the authors' knowledge, development of a theory that accounts for multi-plane energies of interaction is still an open research question.

The principal focus of this study is to provide a better understanding of the mechanisms of colloid retention in porous media that is in agreement across interface-, pore-, and Dacy-scales. Our first aim is to statistically evaluate the contribution of alternative retention sites, beyond the SW, toward particle retention under commonly found environmental conditions. The intent of the present work is to perform an efficient rather than a systematic assessment of the effects of mean pore velocity, saturation, and solution chemistry on the pore-scale locations where particles become immobilized. Our second aim is to assess the impact that dominant retention sites have at other scales of interest in order to justify its consideration in down-/up-scaling modeling efforts. To do this, we determine the spatial distribution of retained colloids from transport experiments that are imaged non-destructively by high resolution XCT. The experimental setup was designed to work with a model porous medium to isolate the role that pore structure plays on filtration. Analyses of the spatial maps are used to simultaneously assess the macroscopic behavior at play, as well as the dominance and saturation of individual retention sites for all pores within the sample. Finally, theoretical particle interactions from xDLVO are used to qualitatively rationalize the observed retention trends.

2. Materials and Methods

2.1. Materials

Custom made hollow glass microspheres coated in a layer of 118 nm silver were used as the silver colloids for experimentation (Microsphere Technology, Limerick, IE). According to the manufacturer, the silver-glass-air spheres have a mean diameter of 14 $\pm$ 4 μm and a density of 1,000 g L^{-1}. Similar particles have been used in previous studies to investigate colloid retention specifically at GG contacts (Li et al., 2006a) and biofilm distribution in porous media (Iltis et al., 2011). Suspensions of 20 g L^{-1} were prepared in the desired background aqueous solution (described below) and used in experiments within 10 hr. Concentrations of metallic silver in waste water are usually below 5 mg L^{-1} (Wielinski et al., 2021). Nonetheless, silver particles are expected to accumulate over time in environmental compartments (Gottschalk et al., 2013), especially with continual application of the nanomaterial source. Metallic silver nanoparticles (Ag-NP) in consumer products have sizes that range between 10 and 100 nm (Kaegi et al., 2011; Tulve et al., 2015; Wielinski et al., 2021), which are smaller than the microspheres used in our experiments. This modification in concentration and particle size from expected values of sludge-receiving soils was required for visualization of deposited material with XCT, as described in Section 2.3.

Borosilicate glass beads of 1 mm mean diameter were used used as the model porous medium (Sigma-Aldrich). The glass beads were chemically pre-treated by soaking in concentrated HCl for 24 hr and rinsing with Milli-Q water until the pH was neutral to remove metal oxides, followed by baking overnight at 550°C to remove organic impurities. The nanoscale surface roughness of glass beads is expected to be small as compared to natural porous media. Thus, both the chemical and physical heterogeneity in the porous medium used for experiments in this work is likely to be small, although not necessarily insignificant. Investigating the level of physicochemical heterogeneity remaining in the already idealized porous medium and its contribution toward immobilization, however, is not explored further. Sandy soils may range in grain size from 0.06 to 2 mm and likely pack differently than the glass bead bed in our experiments. While the particles and porous media used in this study differ in size and packing from the materials expected in real environmental systems, the goal of this work is not to exactly replicate

Table 1
Summary of Experimental Conditions Tested

Label	q [cm h^{-1}]	θ_w/θ [-]	v [cm h^{-1}]	Solution chemistry
A	38.39	1.00, θ_s	71.95, v_f	MQW
B	13.85	0.35, θ_u	82.41, v_f	MQW
C	18.92	1.00, θ_s	34.99, v_s	MQW
D	13.89	0.42, θ_u	69.47, v_f	SDBS
E	13.89	0.41, θ_u	71.16, v_f	DOM

Note. q is the Darcy discharge, θ_w/θ is the fraction of water in the pore space or degree of saturation (where θ is the porosity of the packed bed), with classification into saturated θ_s and unsaturated θ_u. v is the resulting average pore velocity, with classification into fast v_f and slow v_s. Solution chemistry includes Milli-Q Water (MQW), Sodium Dodecylbenzene Sulfonate (SDBS), and Dissolved Organic Matter (DOM).

a natural soil system. Rather, we aim to isolate a problem and disentangle the role that pore structure plays on filtration, which as of yet cannot be investigated in natural samples.

Three different background aqueous solutions were used to vary the particle stability and interface interactions between the silver colloids and the available pore-scale retention sites in the porous medium. The first solution was Milli-Q water (MQW), which was used as the control. The second solution was made with the anionic surfactant sodium dodecylbenzene sulfonate (SDBS) at a concentration of 1% by weight. This surfactant was chosen as representative of laundry formulations (Smulders & Rähse, 2002), thereby simulating the release of silver particles from washed silver impregnated garments. The third solution was made with dissolved organic matter (DOM) at a concentration of 0.02 g L^{-1} as an ubiquitous constituent of soil water and wastewater sludge with known pronounced effects on colloid transport and stability (Abudalo et al., 2010; Bradford, Tadassa, & Pachepsky, 2006; Elimelech et al., 2013; Flury & Qiu, 2008; Granger et al., 2007; Jaisi et al., 2008; Marley et al., 1993; Mibus et al., 2007; Morales, Sang, et al., 2011; Morales, Zhang, et al., 2011; Phenrat et al., 2008; Sen & Khilar, 2006). Specifically, Elliott Soil humic acid (International Humic Substances Society, St. Paul, MN) was used as a standard DOM, following the solution preparation of Morales, Zhang, et al. (2011).

2.2. Column Experiments

Cylindrical polypropylene columns (4.7 mm inner diameter and 35 mm length) were wet-packed to a depth of approximately 30 mm with clean borosilicate glass beads. A piece of stainless steel mesh was placed at the top and bottom of the packed bed to uniformly distribute the liquid at the boundaries and prevent the glass beads from entering the tubing. The flow rate was controlled by a push-pull syringe pump that exactly matched the rate at which influent was dispensed at the top and effluent withdrawn from the bottom of the column. Five pore volumes were used to condition the packed columns with the working background solution prior to transport experiments. Then, a pulse of 400 µL of the colloidal suspension was injected at a continuous flow rate, followed by flushing with particle-free background solution until the effluent concentration returned to baseline levels. The effluent concentration was measured in a flow-through cuvette by UV-vis spectrophotometry at a wavelength of 600 nm in 30 s intervals. Particle concentration in the effluent was determined from established linear calibration curves. Following the experiment, the column was sealed at both ends to prevent evaporation, maintained in a vertical position, and immediately analyzed with tomographic imaging on site, to ensure relocation did not change particle deposition patterns.

Replicate experiments were conducted for variable conditions regarding: (a) water content (saturated vs. unsaturated), (b) pore velocity (fast vs. slow), and (c) solution chemistry (MQW vs. SDBS vs. DOM) as summarized in Table 1. Saturated conditions required inlet/outlet flow rates to always remain matched after wet packing the column. To achieve unsaturated conditions, the inlet and outlet flow rates were temporarily mismatched (the inlet flow was reduced) to allow for slow draining. When the desired water content was reached (determined gravimetrically), matching of inflow and outflow rates was resumed and allowed to equilibrate prior to injection of the particle suspension. It is important to note that unsaturated experiments experienced a gradient in moisture content with depth, as illustrated in Figure S2 in Supporting Information S1, which is extremely difficult to overcome for such small columns. The water content of each packed column was measured before and after the transport experiment to verify that it remained constant. Only experiments that met a constant water content condition were considered here. The pore velocity, $v = q/\theta_w$, was controlled through the imposed Darcy discharge, $q = Q/A$, and the volumetric water content of each experiment, θ_w, where Q is the flow rate and A is the cross-sectional area of the column. The solution chemistry was maintained constant throughout each experiment, whereby the background solution for the suspension and the particle-free solution used to flush out the colloid pulse were the same.

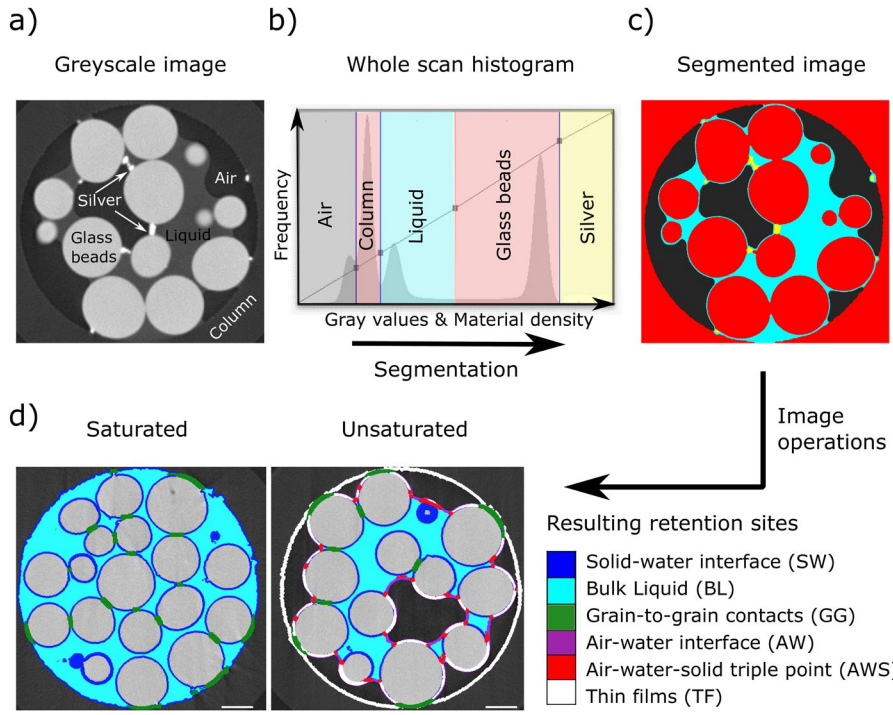

Figure 1. Workflow used to define pore-scale retention sites: (a) cross section of X-ray computed tomography (XCT) images in greyscale, (b) histogram showing the peak cutoffs used to distinguish each bulk material, (c) image segmentation of bulk phases in false coloring, (d) cross section of XCT images illustrating the six different retention site region of interests in false coloring for saturated (L) and unsaturated (R) experiments. The scale bar represents 500 μm.

2.3. XCT Scanning and Enumeration of Retained Particles

XCT scanning: XCT imaging of the column was conducted with a bench-top scanner (HMX Nikon Metrology, Derby, UK) to obtain a detailed three-dimensional static picture of the distribution of retained colloids in the porous medium. To achieve a voxel resolution of ~10 μm, the sample was scanned in two separate segments of ~15 mm length. The X-ray source was set to an energy of 50 kV with 300 μA intensity. A 0.1 mm aluminum filter was used to reduce beam-hardening artifacts. A complete 360° scan consisted of 2,000 projections, with two frames per projection. Image reconstruction was performed with the scanner's designated software, CT-Pro. Details about the optimized XCT scanning settings are provided in the Supporting Information S1 (SI).

Segmentation: Image segmentation was used to define the different materials in each column with dedicated commercial software for XCT image analysis (VG Studio Max 2.1, Heidelberg, DE). First, the images were pre-processed using a non-local mean filter to increase the signal-to-noise ratio. Adaptive thresholding was then used to segment the bulk phases with operator-specified input parameters for the *solids* (glass beads ∪ column), *water*, and *air* (for partly water saturated experiments). Region grower was used to refine particularly noisy bulk phase segmentation results. Finally, global thresholding was used again to segment total retained *silver colloids*, as the sample material with highest X-ray attenuation and largest histogram gray values. It is worth noting that the experimental materials were deliberately chosen to simplify their segmentation based on well-defined histogram peak cutoffs as illustrated in Figure 1. The SI describes the control tests performed to determine the visibility of retained colloids in the column.

Three-dimensional regions of interest (ROIs) for each prospective retention site were defined using a sequence of image operations (union, dilation, intersection, and difference) on the defined bulk phase elements as follows. First, the *solids*, *water* and *air* elements were dilated by 2 voxels, here denoted by the subscript *d*. Next, the intersection between dilated element pairs $solids_d \cap water_d$, $air_d \cap water_d$, and $air_d \cap solids_d$ were used to create new elements corresponding to interfaces with the *solid-water* (SW), *air-water* (AW), and *air-solid* (TF, which refers to thin films), respectively. The *air-water-solid* (AWS) triple point element was defined as the intersection

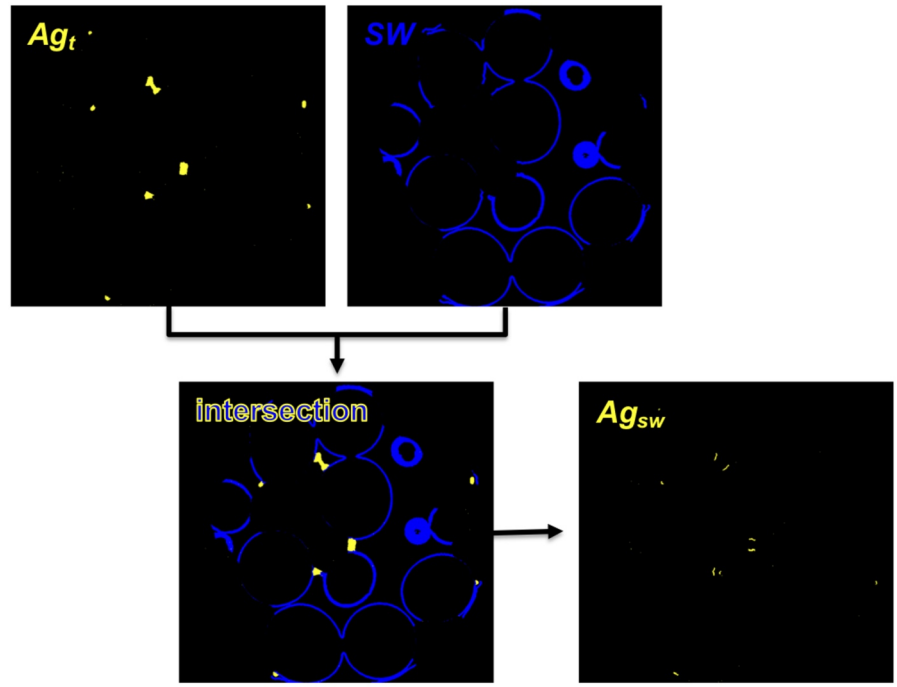

Figure 2. Exemplary intersection operation between elements for total retained silver (Ag_T) and a pore-scale retention site (solid-water interface, SW) at a given depth z. The outcome is retention site-specific silver accumulation, here silver retained at the solid-water interface (Ag_{SW}).

between $solids_d$, $water_d$ and air_d. The *grain-to-grain* (GG) contact element was obtained from watershed lines of the *solid* element. Then, all retention site elements were dilated by two voxels to create true volumes of otherwise two-dimensional surfaces. This initial definition of elements (i.e., ROIs that delineate the six pore-scale retention sites) causes them to overlap in some portions of the image volume. Subtraction of elements from one another is then used to assign voxels to only one retention site ROI. Lastly, a *bulk liquid* (BL) element was defined as the difference between the *water* element and all retention sites. This site would capture any retained silver mass that might protrude into the bulk water by straining. To summarize, we detect ROIs corresponding to six types of retention size, $\mathcal{S} = \{\text{SW, BL, GG, AW, AWS, TF}\}$. Figure 1 illustrates in false coloring the ROIs for each retention site available for a saturated and an unsaturated column.

2.4. Depth Profiles and Retention Site Statistics

ROIs belonging to total retained silver (Ag_T) and each individual prospective retention site $i \in \mathcal{S}$ were processed in pairs with the intersection operation to deduce the quantity of silver colloids deposited at each site, Ag_i. Figure 2 illustrates this process for silver retained at the SW interface at a given depth, z. These values were subsequently used to obtain (a) retention site-dependent depth profiles (Darcy-scale) and (b) the fraction of retained silver in each site to determine their dominance and saturation (pore-scale). To the author's knowledge, this is the first attempt to extract quantitative information relating colloid immobilization to pore-scale retention sites from three-dimensional information of the structure and deposition patterns of a filter medium.

Tomographic images of each experiment described in Table 1 contained N cross sections in depth. Each two-dimensional section, n, had a thickness of ~10 μm, corresponding to a voxel length Δz. From these data, depth profiles of total silver were extracted, $Ag_T(z)$. The fraction of total retained silver found at each site in a given image cross section, m_i, is given by $m_i(n) = Ag_i(n)/Ag_T(n) = \frac{1}{\Delta z}\int_{\Delta z\cdot(n-1)}^{\Delta z\cdot n} \frac{Ag_i(z)}{Ag_T(z)}\,dz$. To rank the sites by importance, dominance was measured as the mean fraction of retained silver for a given retention site as:

$$\overline{m}_i = \frac{\sum_{n=1}^{N} m_i(n)}{N} \tag{1}$$

To translate findings to systems with different retention site proportions, knowledge about the fullness of each site is needed. The fraction of retention site volume i filled with silver in a given image cross section, f_i, is given by $f_i(n) = Ag_i(n)/V_i(n) = \frac{1}{\Delta z}\int_{\Delta z\cdot(n-1)}^{\Delta z\cdot n} \frac{Ag_i(z)}{V_i(z)} dz$. Site saturation was then measured as the mean normalized fraction of retained silver by retention site volume as:

$$\overline{f}_i = \frac{\sum_{n=1}^{N} f_i(n)}{N} \tag{2}$$

It is noteworthy that the site ROIs can be composed of multiple objects (discontinuous clusters of voxels, e.g., the GG ROI is composed of multiple individual GG contacts), where each object can retain different quantities of silver particles. This is inevitable, yet $\overline{f}_i$ summarizes how full the collection of those objects is with retained colloids and allows us to compare against other retention sites i.

2.5. Interaction Energy Profiles

Surface interactions for colloids approaching other charged surfaces were determined by extended-DLVO theory and parametrized by the system's physico-chemical properties listed in Table S2 in Supporting Information S1. The sum of van der Waals (V_{VDW}), electric double layer interactions (V_{EDL}), steric interactions (V_{ST}), and Lewis acid-base interactions (V_{AB}) are considered for colloid-SW and colloid-colloid systems (Butt et al., 2005; Elimelech et al., 2013; Grabbe, 1993; Gregory, 1981; Lin & Wiesner, 2012; Wood & Rehmann, 2014). Colloid-colloid interactions were used to assess the likelihood for accumulation of colloids at close proximity in GG contacts and AWS triple points. Additionally, hydrophobic interactions (V_{HYD}) are taken into account for the colloid-AW system (Yoon & Mao, 1996). There is not a proper interaction energy scheme to describe colloids approaching the TF which is why their profiles are excluded from this analysis.

The analytical expressions for the various interactions considered (in sphere-sphere geometry) are given by the following:

$$V_{VDW} = -\frac{A}{6D}\left(\frac{R_1 R_2}{R_1 + R_2}\right)\left[1 - \frac{5.32D}{\lambda}\ln\left(1 + \frac{\lambda}{5.32D}\right)\right] \tag{3}$$

$$V_{EDL} = 64\pi\epsilon\left(\frac{R_1 R_2}{R_1 + R_2}\right)\left(\frac{\kappa_B T}{\nu e}\right)^2 \tanh\left(\frac{\nu e\zeta_1}{4\kappa_B T}\right)\tanh\left(\frac{\nu e\zeta_2}{4\kappa_B T}\right)e^{-\kappa D} \tag{4}$$

$$V_{ST} = \pi a_{ST}^2 \gamma_0^{ST} \exp\left(-\frac{D}{\lambda_{ST}}\right) \tag{5}$$

$$V_{AB} = 2\pi R_1 \lambda_{AB}\gamma_0^{AB}\left[1 - \frac{\lambda_{AB}}{R_1} + \left(1 + \frac{\lambda_{AB}}{R_1}\right)e^{-\frac{2R_1}{\lambda_{AB}}}\right]\exp\left(-\frac{D}{\lambda_{AB}}\right) \tag{6}$$

$$V_{HYD} = -\frac{K_{HYD}}{6D}\left(\frac{R_1 R_2}{R_1 + R_2}\right) \tag{7}$$

here, A is the Hamaker constant for the system, D is the separation distance, R_1 and R_2 are the radii of two interacting spheres. For colloid-colloid interactions $R_1 = R_2 = 7$ μm. For colloid-SW and colloid-AW $R_1 = 7$ μm and $R_2 = \infty$. λ, λ_{ST}, and λ_{AB} are the decay length for van der Waals, steric and Lewis acid-base interactions, respectively. ϵ is the dielectric constant of the water, κ_B is the Boltzmann constant, T is temperature, ν is the valence of the symmetric electrolyte, e the charge of an electron, ζ_1 and ζ_2 are the zeta potential of the two interacting materials. κ is the inverse Debye length, a_{ST} is the radius of steric hydration contact. K_{HYD} is the hydrophobic constant for air bubbles interacting with silver particles in water, here estimated as 7.67×10^{-20}.

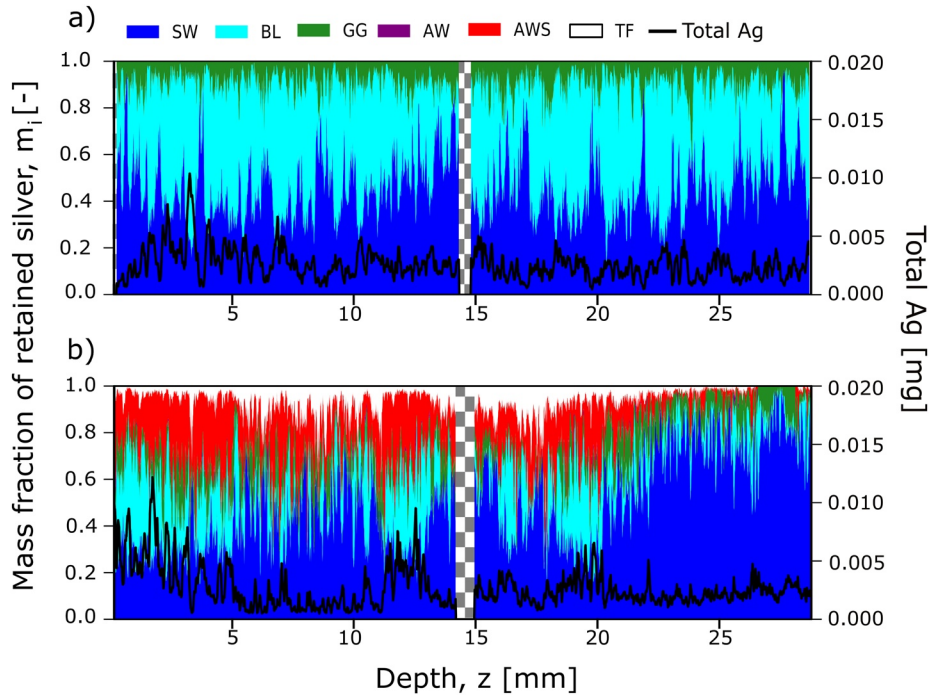

Figure 3. Depth profiles. Primary *y*-axis shows stacked area plots of the fraction of retained silver at six candidate pore sites with depth. Secondary *y*-axis shows the total retained silver with depth (black line). A comparison is presented for experiments of constant pore velocity (v_f) and solution chemistry (MQW) but variable water content: (a) fully saturated (θ_s), (b) unsaturated (θ_u). Checkered shading indicates missing data during image stitching. The fraction of retained colloids at each site is relatively constant in depth, while the total mass of silver retained changes non-monotonically with depth.

3. Results and Discussion

3.1. Darcy-Scale Fate and Transport

Mass balance of silver eluted from each experiment revealed that, on average, <10% of the applied silver mass was recovered in the effluent for all tested conditions (See Table S3 in Supporting Information S1). Such low mobility is consistent with previous studies on transport of silver particles in neutral to alkaline conditions (Rahmatpour et al., 2018) and is expected for transport of large-sized particles (>1 μm in diameter, as are the size of our particles; Molnar, Johnson, et al., 2015). Here, we exploit the high degree of retention to cross-examine deposition patterns.

Depth profiles of retained particles in experiments testing variable water content are shown in Figure 3. The primary *y*-axis shows a stacked area plot of the fraction of silver particles deposited by available retention site in depth. The secondary *y*-axis shows the classic depth profile as the total mass of silver retained in depth. Similar profiles corresponding to experiments comparing pore velocity and solution chemistry are provided in Figures S3 and S4 in the Supporting Information S1, respectively. The large signal variability is due to the high data resolution, given that depth intervals are collected at 10 μm from XCT imaging rather than the 1 cm from standard destructive approaches. Depth profiles from replicate experiments are in qualitative agreement, but only representative results are presented for the purpose of comparison.

Close inspection of Figure 3 reveals two important trends. First, the contribution order toward retention by each prospective site (staked areas) is relatively uniform along the column depth. Even though there is high variability in the signal, there is no cross over of site dominance as a function of depth. This suggests that available sites, however small they are, have not become entirely saturated. In water saturated conditions, the mass of immobilized particles is distributed between three retention sites with substantial contribution from sites other than the SW interface. In water unsaturated conditions, similar trends are observed, albeit with additional retention sites available. The slight change in retained particle distribution in the last 10 mm of the column can be explained by a modest increase in saturated at the lower boundary (Leuther et al., 2020). In both water saturation systems the

SW interface contributes significantly, though not exclusively to particle retention. Knowledge of the identity and relative contribution of active retention sites is critical for improving mechanistic models for colloid filtration. In the following section we discuss the specific contribution by each retention site.

Second, the depth profiles of total mass of silver (black solid line) are non-monotonic and characteristic of *anomalous* transport (the reader is additionally referred to Figure S5 in Supporting Information S1 for a moving average of the same signal). *Normal* colloid transport follows an exponential decay in mass retained with depth; thereby any departure from this is considered anomalous. Similar anomalous trends in depth were observed for experiments of variable pore water velocity and pore water chemistry (Figures S3 and S4 in Supporting Information S1). Specifically, non-monotonic deposition has been ascribed to non-attached colloids in the near surface domain (Johnson et al., 2018) that may accumulate at hydrodynamically stagnant regions. This mechanistic perception is in agreement with observed accumulation of particles at all depths in GG contacts for the saturated case and AWS triple points for the unsaturated case. Importantly, distinguishing between the mass retained at perfect sinks (SW with infinite retention time) and imperfect sinks (flow stagnation regions of GG or AWS with finite retention time) can help better understand the mechanisms leading to breakthrough curves with heavy tailing. Modeling broad residence time distributions is yet subject of future work.

In all experiments, particles remained at the BL even after flushing for more than 10 pore volumes likely because, even in a bead pack, the flow field is not perfectly homogeneous (Morales et al., 2017) and flow-induced aggregation created particle clusters that were too large to be flushed out (Perez et al., 2020). Additional tests were conducted in transient conditions for draining (data not shown) that eluted material retained at the BL, thus confirming that the image signal at this location is truthful.

3.2. Pore-Scale Retention Site Statistics

Mean site dominance $\left(\overline{m}_i\right)$, and mean site saturation $\left(\overline{f}_i\right)$ results are presented as scatter clusters in Figure 4. It is worth noting that by definition, $\overline{m}_i$ adds up to unity because it is normalized by the total silver immobilized throughout the column and summarizes the overall site contribution toward particle immobilization. On the other hand, the mean site saturation $\overline{f}_i$ depends on the unique volume of available retention site i and does not need to add up to unity. Subfigures are organized to facilitate comparisons for variable water content (Figures 4a and 4d), variable pore velocity (Figures 4b and 4e), and variable solution chemistry (Figures 4c and 4f). The reader is referred to Table 1 for the other conditions maintained constant for each grouping.

General: Across all experiments, the SW interface (blue markers) was the most dominant retention site (highest $\overline{m}_i$ values) but accounted only for up to half of the total mass retained ($\overline{m}_{SW} \leq 0.5$), while the AW and TF were the least dominant retention sites $\left(\overline{m}_{AW} | \overline{m}_{TF} \leq 0.15\right)$. This implies that mechanistic models should account for multiple sinks terms to more accurately represent the processes involved in anomalous colloid filtration behavior. Regarding site saturation, no site ever approached its full capacity $\left(\overline{f}_i < 3 \times 10^{-3}\right)$, however small they were. These outcomes are expected because saturation of a retention site is never anticipated to be complete unless the deposition conditions are fully favorable. This is not the case for any of the experimental conditions in this study. For this and various additional reasons, deposition in a given retention site is hindered, and thus the quantity $\overline{f}_i$ can be limited to a maximum which is lower than unity. Additionally, this suggests that it is unlikely that primary retention would switch from one site to another upon reaching a threshold saturation.

Variable water content: For variable water content, Figure 4a shows that the stagnant regions, represented by the GG contacts in saturated and GG plus AWS in unsaturated experiments, are responsible of at least 0.1 of the total mass retained. The BL is the second most dominant site in both saturated and unsaturated conditions, but there is a decrease in $\overline{m}_{BL}$ with decreasing water content. The value of $\overline{m}_{AWS}$ for unsaturated conditions suggests a trade-off of deposited particles between the BL and the stagnant region AWS when the system goes from saturated to unsaturated conditions.

Regarding the site saturation (Figure 4d), AWS has the highest value of $\overline{f}_i$ for unsaturated conditions, which means that this site is the most saturated with particles, followed by the SW. In saturated conditions, the GG showed higher $\bar{f}_i$ than the BL, but the most filled up site with particles was the SW. One can conjecture from these data that, when present, AWS sites affect the flow field more strongly than GG contacts between perfectly spherical grains.

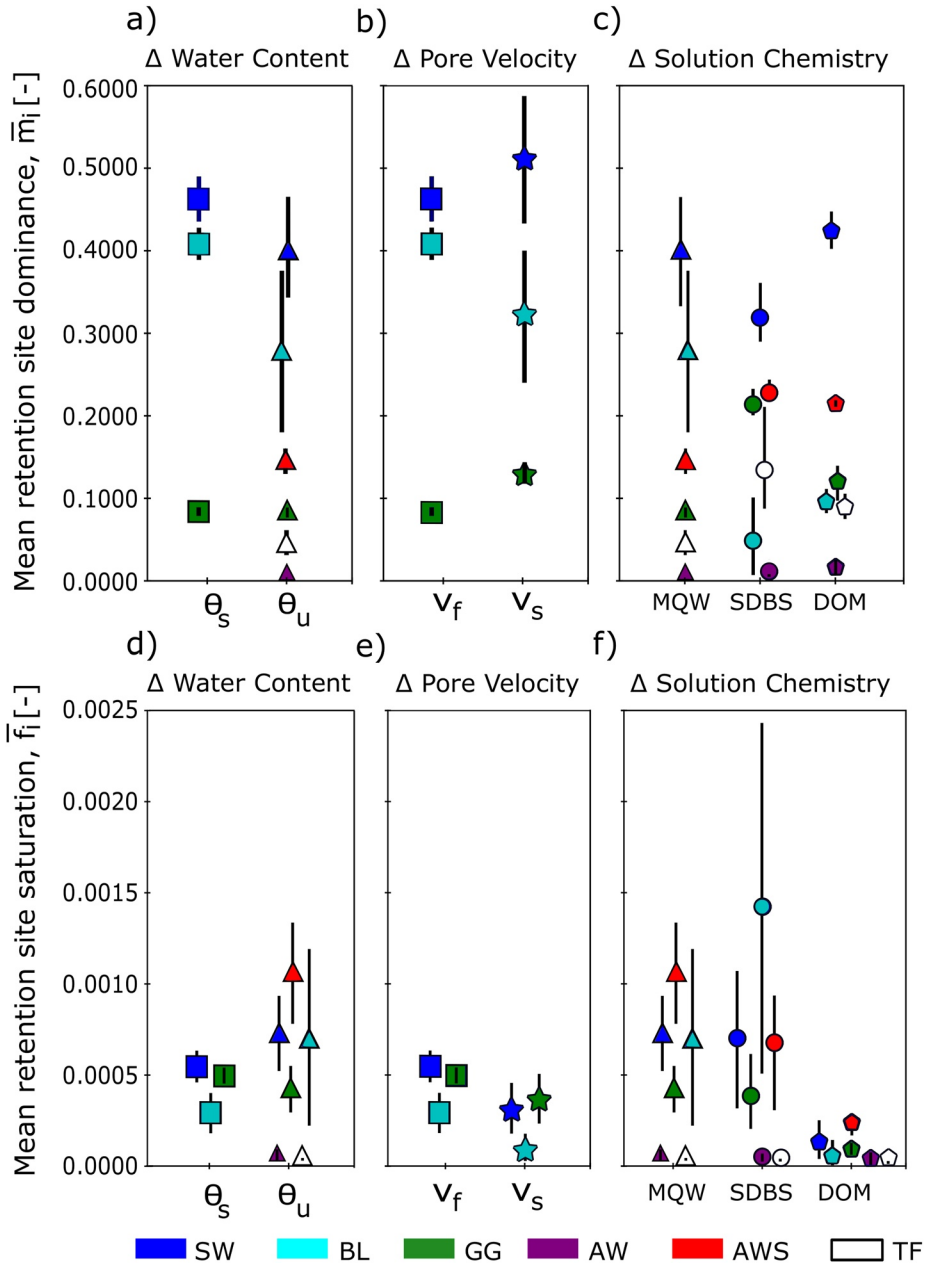

Figure 4. (Top) Mean retention site dominance, $\overline{m}_i$, and (bottom) mean retention site saturation, $\overline{f}_i$, for experiments of variable (a, d) water content (b, e) pore velocity, and (c, f) solution chemistry. Error bars denote maximum and minimum values for replicate experiments. Retention sites considered are solid-water interface (SW), grain-to-grain contacts (GG), bulk liquid (BL), air-water interface (AW), air-water-solid triple points (AWS), and thin films (TF). The most dominant site for silver retention is the SW, with flow-stagnant regions (GG for saturated and AWS for unsaturated experiments) following closely behind in all experiments. The AW ranked last in dominance whenever present. The site saturation of flow-stagnant regions is comparable to, and at times higher than, the SW. The AW and TF rank lowest for saturation whenever present.

Variable pore velocity: The dominance of the retention sites was similar for variable pore velocity, Figure 4b. Nonetheless, it is worth noting that both $\overline{m}_{SW}$ and $\overline{m}_{GG}$ increased with decreasing v. This observed behavior can be explained by longer contact times between particles and the SW, and longer particle residence times in the stagnation regions when the flow rate/mean pore velocity is lower (Li et al., 2006b).

The SW saturation ($\overline{f}_{SW}$) was comparable to the one of GG ($\overline{f}_{GG}$) when pore velocity was reduced, pointing to a larger proportion of retention at the flow stagnation zones of the system—GG contacts under lower pore

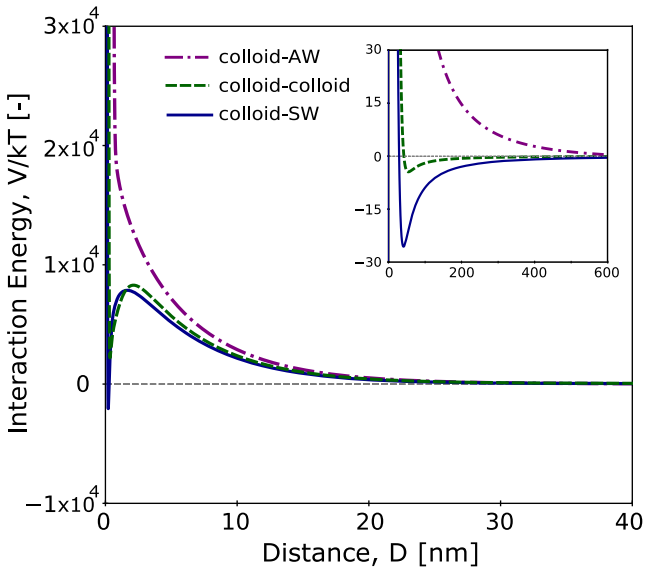

Figure 5. Total interaction energy as a function of separation distance for colloids approaching different charged surfaces: solid-water interface (SW), air-water interface (AW), and another colloid. Inset shows the secondary energy minima. The lowest energy barrier and deepest secondary energy well for the colloid-SW interactions are in agreement with the observed dominance of retention at the SW. A similar barrier and slightly more shallow secondary well for colloid-colloid interactions suggest weak aggregation and support the significant particle accumulation at flow-stagnant regions pertaining to grain-to-grain contacts and the air-water-solid triple point. The highest energy barrier and no secondary well for colloid-AW interactions support observations of minimal particle retention at the AW.

velocities (see Figure 4e). These outcomes are in agreement with detailed studies of the inversely proportional size of flow stagnation zones with flow rate/pore velocity (Johnson et al., 2007). For the system under investigation, this amounts to larger stagnant flow regions associated with GG contacts at slower pore water velocities, leaving thereby fewer colloids to be retained at the SW interface and the BL.

Variable solution chemistry: For variable solution chemistry, the second most dominant site changes from BL in simple solutions (MWQ) to flow stagnation regions associated with the AWS and GG for more complex solutions (SDBS and DOM; see Figure 4c). Under all tested solution chemistries, the AW and TF ranked at the bottom of the list for site dominance, hinting that the importance of the AW in unsaturated media is less prominent than has been suggested in the literature. The authors conjecture that the reasoning postulated by Bradford and Torkzaban (2008) explains this observation. In short, near perfect slip conditions at the AW interface results in colloids sliding along the surface of air bubbles, directing them to AWS where they can more permanently arrest.

Site saturation in Figure 4f was greatest for the SW and AWS interfaces. The large variability observed for $\overline{f}_{BL}$ in different treatments makes it difficult to draw general claims about its likelihood to fill up. Similarities in the $\overline{m}_i$ and $\overline{f}_i$ trends across solution chemistries, exclusive of the BL, suggest that changes in the interaction energy between colloids and available charged surfaces were not significantly affected by the presence of surface active compounds.

3.3. Interface-Scale Interaction Energy

Energy profiles for a colloid interacting with: the SW interface (solid line), the AW interface (dot-dashed line), and another colloid (dashed line) in MQW solution chemistry are shown in Figure 5. Interactions between colloids and the SW interface are characterized by the lowest energy barrier ($\sim 7.5 \times 10^3\ kT$) coupled with the deepest secondary energy well ($\sim -25\ kT$). These conditions are considered relatively *favorable* for reversible deposition at this retention site. Similar interactions were found between identical colloids (i.e., for flocculation) with a low energy barrier ($\sim 8 \times 10^3\ kT$) and a slightly more shallow secondary energy well ($\sim -5\ kT$). These conditions too are considered *favorable* for accumulation of colloids at close proximity in stagnant flow regions. Interactions between colloids and the AW interface involve the highest determined energy barrier ($\sim 3 \times 10^4\ kT$) and an absent secondary energy minimum. Such conditions are typified highly *unfavorable*.

On the basis of interaction energy profiles, silver particles are expected to (a) deposit at the SW interface, albeit at the secondary minimum; (b) aggregate (including weak flocculation) with comparable proportion at either GG contacts or AWS, depending on the system's water saturation as discussed above, or protruding into the BL; and (c) never deposit at the AW interface. These interface-scale energetic trends are in agreement with observations of pore-scale site dominance and saturation shown in Figure 4 and Darcy-scale depth profiles shown in Figure 3, showing consistency across scales of investigation.

The authors note that the magnitude of the energy barrier height ($\gg \mathcal{O}\left(10^3\right)$ kT) for all computed interactions is insurmountable and implies that retention at a primary well is extremely unlikely. This is in agreement with the work by Shen et al. (2007), who report a lack for primary minimum interaction for particles larger than 1 μm. In addition, the high degree of particle deposition observed across all experiments suggests that surface heterogeneity on the collector surface may have remained even after efforts to minimize it. While interactions between colloids and nanoscale heterogeneities on the collector surface can be *locally* highly favorable, theoretical interactions based on bulk measurements, as those shown in Figure 5, suggest *effective* unfavorable interactions for the system as a whole. That is, the interaction between a colloid and the heterogeneous collector surface is *on average* highly unfavorable. For the work here presented, the physico-chemical heterogeneity was removed as much as possible through synthetic manufacturing of smooth glass beads and chemical and thermal treatment. Yet, it is

difficult to ascertain empirically if any level of heterogeneity remained that contributed to retention. The xDLVO profiles of Figure 5 show highly unfavorable effective interactions, yet significant retention was observed. We primarily ascribe this to secondary minimum interactions and pore-structure, but cannot rule out that some level of heterogeneity on the flat interfaces also impacted retention.

When considering heterogeneity more explicitly, colloids are expected to stochastically interact with portions of the collector surface that are entirely within, partially on, or entirely outside a heterogeneous nanosite (Ron & Johnson, 2020). These possibilities produce interactions that are favorable, intermediately favorable, or unfavorable, respectively, and cannot be inferred from effective xDLVO profiles. Hence, the authors suggest that a more appropriate representation of colloid-collector interactions in the presence of heterogeneity would honor the variability of possible interactions. However, investigating more deeply the impact of surface heterogeneity on xDLVO energy profiles and ultimately on upscaled particle transport models is the subject of future work.

4. Conclusions

This study demonstrates that colloid deposition at the Darcy-, pore- and interface- scales are in full agreement when the pore structure is taken into account. At the Darcy-scale, transport was deemed consistently anomalous based on non-monotonic depth profiles observed, which are affected by regions of low-flow. Detailed analysis of retention site-specific depth profiles revealed that immobilized colloids were distributed broadly across six candidate retention-sites, and that the distribution was consistent in depth and largely independent of the experimental conditions tested. At the pore-scale, analysis of deposited mass identified the solid-water interface as the dominant retention site in all tested conditions, but it only retained up to 0.5 of the total deposited mass. Significant retention was additionally found in flow-stagnant regions corresponding to grain-to-grain contacts and the air-water-solid triple point for saturated and unsaturated systems, respectively. In unsaturated systems, deposition at the air-water interface was minimal. At the interface-scale, interaction energy profiles were in excellent consonance with the dominance ranking of available retention sites. Attachment to the solid-water interface and weak aggregation (in low-flow regions) were found to be favorable, while attachment to the air-water interface was deemed highly unfavorable. While the idealized colloids and porous media used in this work are a simplification of complex environmental systems, the findings reported shed light on the fundamental role that pore structure in aquifer media plays on the immobilization of suspended groundwater contaminants. Future work with more realistic materials and larger experimental columns would increase the representativeness of the results for real environmental systems. Significant retention of colloids in flow stagnation zones, which are subject to reentrainment by diffusive means, is likely a key driver of ubiquitous heavy tails in breakthrough curves. Understanding the physical justification for colloid elution (e.g., long residence times vs. detachment kinetics) is critical to revise mechanistic models that can more accurately predict fate and transport under environmentally relevant transient conditions.

Data Availability Statement

The data for depth profiles of retained particles and retention site distribution are available at https://doi.org/10.5281/zenodo.6456378.

Acknowledgments
This work was supported in part by the U.S. National Science Foundation (EAR-1847689), the Donors of the American Chemical Society Petroleum Research Fund (59864-DNI9), and Marie Curie Actions (FP7-PEOPLE-2012-Soil-ArchnAg No. 302251). The authors thank the Editor Kamini Singha and three anonymous reviewers for their thorough and constructive feedback.

References

Abudalo, R., Ryan, J., Harvey, R. W., Metge, D. W., & Landkamer, L. (2010). Influence of organic matter on the transport of Cryptosporidium parvum oocysts in a ferric oxyhydroxide-coated quartz sand saturated porous medium. *Water Research*, *44*(4), 1104–1113. https://doi.org/10.1016/j.watres.2009.09.039

Adamczyk, Z., Siwek, B., Zembala, M., & Belouschek, P. (1994). Kinetics of localized adsorption of colloid particles. *Advances in Colloid and Interface Science*, *48*, 151–280. https://doi.org/10.1016/0001-8686(94)80008-1

Babakhani, P., Bridge, J., Doong, R.-a., & Phenrat, T. (2017). Continuum-based models and concepts for the transport of nanoparticles in saturated porous media: A state-of-the-science review. *Advances in Colloid and Interface Science*, *246*, 75–104. https://doi.org/10.1016/j.cis.2017.06.002

Benn, T., Cavanagh, B., Hristovski, K., Posner, J. D., & Westerhoff, P. (2010). The release of nanosilver from consumer products used in the home. *Journal of Environmental Quality*, *39*(6), 1875–1882. https://doi.org/10.2134/jeq2009.0363

Benn, T., & Westerhoff, P. (2008). Nanoparticle silver released into water from commercially available sock fabrics. *Environmental Science & Technology*, *42*(11), 4133–4139. https://doi.org/10.1021/es7032718

Bergendahl, J., & Grasso, D. (1998). Colloid generation during batch leaching tests: Mechanics of disaggregation. *Colloids and Surfaces A: Physicochemical and Engineering Aspects*, *135*(1–3), 193–205. https://doi.org/10.1016/s0927-7757(97)00248-3

Birdi, K. S. (2008). *Handbook of surface and colloid chemistry*. CRC press.
Bradford, S. A., & Bettahar, M. (2005). Straining, attachment, and detachment of Cryptosporidium oocysts in saturated porous media. *Journal of Environmental Quality*, *34*(2), 469–478. https://doi.org/10.2134/jeq2005.0469
Bradford, S. A., Simunek, J., Bettahar, M., Van Genuchten, M. T., & Yates, S. (2006). Significance of straining in colloid deposition: Evidence and implications. *Water Resources Research*, *42*(12). https://doi.org/10.1029/2005wr004791
Bradford, S. A., Tadassa, Y. F., & Pachepsky, Y. (2006). Transport of Giardia and manure suspensions in saturated porous media. *Journal of Environmental Quality*, *35*(3), 749–757. https://doi.org/10.2134/jeq2005.0226
Bradford, S. A., & Torkzaban, S. (2008). Colloid transport and retention in unsaturated porous media: A review of interface-collector-and pore-scale processes and models. *Vadose Zone Journal*, *7*(2), 667–681. https://doi.org/10.2136/vzj2007.0092
Bradford, S. A., Torkzaban, S., & Walker, S. L. (2007). Coupling of physical and chemical mechanisms of colloid straining in saturated porous media. *Water Research*, *41*(13), 3012–3024. https://doi.org/10.1016/j.watres.2007.03.030
Butt, H.-J., Cappella, B., & Kappl, M. (2005). Force measurements with the atomic force microscope: Technique, interpretation and applications. *Surface Science Reports*, *59*(1–6), 1–152. https://doi.org/10.1016/j.surfrep.2005.08.003
Chen, G., & Flury, M. (2005). Retention of mineral colloids in unsaturated porous media as related to their surface properties. *Colloids and Surfaces A: Physicochemical and Engineering Aspects*, *256*(2–3), 207–216. https://doi.org/10.1016/j.colsurfa.2005.01.021
Chen, G., Liu, X., & Su, C. (2011). Transport and retention of TiO_2 rutile nanoparticles in saturated porous media under low-ionic-strength conditions: Measurements and mechanisms. *Langmuir*, *27*(9), 5393–5402.
Cortis, A., Harter, T., Hou, L., Atwill, E. R., Packman, A. I., & Green, P. G. (2006). Transport of Cryptosporidium parvum in porous media: Long-term elution experiments and continuous time random walk filtration modeling. *Water Resources Research*, *42*(12). https://doi.org/10.1029/2006wr004897
Crist, J. T., McCarthy, J. F., Zevi, Y., Baveye, P., Throop, J. A., & Steenhuis, T. S. (2004). Pore-scale visualization of colloid transport and retention in partly saturated porous media. *Vadose Zone Journal*, *3*(2), 444–450. https://doi.org/10.2113/3.2.444
Crist, J. T., Zevi, Y., McCarthy, J. F., Throop, J. A., & Steenhuis, T. S. (2005). Transport and retention mechanisms of colloids in partially saturated porous media. *Vadose Zone Journal*, *4*(1), 184–195. https://doi.org/10.2136/vzj2005.0184
Derjaguin, B. V. (1941). *Acta Physicochim* (Vol. 14). USSR.
Dimkpa, C., Calder, A., Gajjar, P., Merugu, S., Huang, W., Britt, D., et al. (2011). Interaction of silver nanoparticles with an environmentally beneficial bacterium, Pseudomonas chlororaphis. *Journal of Hazardous Materials*, *188*(1–3), 428–435. https://doi.org/10.1016/j.jhazmat.2011.01.118
El Badawy, A. M., Silva, R. G., Morris, B., Scheckel, K. G., Suidan, M. T., & Tolaymat, T. M. (2011). Surface charge-dependent toxicity of silver nanoparticles. *Environmental Science & Technology*, *45*(1), 283–287. https://doi.org/10.1021/es1034188
Elimelech, M., Gregory, J., & Jia, X. (2013). *Particle deposition and aggregation: Measurement, modelling and simulation*. Butterworth-Heinemann.
Elimelech, M., & O'Melia, C. R. (1990). Kinetics of deposition of colloidal particles in porous media. *Environmental Science & Technology*, *24*(10), 1528–1536. https://doi.org/10.1021/es00080a012
Flury, M., & Qiu, H. (2008). Modeling colloid-facilitated contaminant transport in the vadose zone. *Vadose Zone Journal*, *7*(2), 682–697. https://doi.org/10.2136/vzj2007.0066
Gajjar, P., Pettee, B., Britt, D. W., Huang, W., Johnson, W. P., & Anderson, A. J. (2009). Antimicrobial activities of commercial nanoparticles against an environmental soil microbe, Pseudomonas putida KT2440. *Journal of Biological Engineering*, *3*(1), 1–13. https://doi.org/10.1186/1754-1611-3-9
Gao, B., Steenhuis, T. S., Zevi, Y., Morales, V. L., Nieber, J. L., Richards, B. K., et al. (2008). Capillary retention of colloids in unsaturated porous media. *Water Resources Research*, *44*(4). https://doi.org/10.1029/2006wr005332
Geranio, L., Heuberger, M., & Nowack, B. (2009). The behavior of silver nanotextiles during washing. *Environmental Science & Technology*, *43*(21), 8113–8118. https://doi.org/10.1021/es9018332
Goldberg, E., Scheringer, M., Bucheli, T. D., & Hungerbühler, K. (2014). Critical assessment of models for transport of engineered nanoparticles in saturated porous media. *Environmental Science & Technology*, *48*(21), 12732–12741. https://doi.org/10.1021/es502044k
Goswami, L., Kim, K.-H., Deep, A., Das, P., Bhattacharya, S. S., Kumar, S., & Adelodun, A. A. (2017). Engineered nano particles: Nature, behavior, and effect on the environment. *Jounal of Environmental Management*, *196*, 297–315. https://doi.org/10.1016/j.jenvman.2017.01.011
Gottschalk, F., Sun, T., & Nowack, B. (2013). Environmental Concentrations of engineered nanomaterials: Review of modeling and analytical studies. *Environmental Pollution*, *181*, 287–300. https://doi.org/10.1016/j.envpol.2013.06.003
Grabbe, A. (1993). Double layer interactions between silylated silica surfaces. *Langmuir*, *9*(3), 797–801. https://doi.org/10.1021/la00027a032
Granger, S., Bol, R., Butler, P., Haygarth, P., Naden, P., Old, G., et al. (2007). Processes affecting transfer of sediment and colloids, with associated phosphorus, from intensively farmed grasslands: Tracing sediment and organic matter. *Hydrological Processes: International Journal*, *21*(3), 417–422. https://doi.org/10.1002/hyp.6597
Gregory, J. (1981). Approximate expressions for retarded van der Waals interaction. *Journal of Colloid and Interface Science*, *83*(1), 138–145. https://doi.org/10.1016/0021-9797(81)90018-7
Hadrup, N., & Lam, H. R. (2014). Oral toxicity of silver ions, silver nanoparticles and colloidal silver–a review. *Regulatory Toxicology and Pharmacology*, *68*(1), 1–7. https://doi.org/10.1016/j.yrtph.2013.11.002
Hedberg, J., Lundin, M., Lowe, T., Blomberg, E., Wold, S., & Wallinder, I. O. (2012). Interactions between surfactants and silver nanoparticles of varying charge. *Journal of Colloid and Interface Science*, *369*(1), 193–201. https://doi.org/10.1016/j.jcis.2011.12.004
Iltis, G. C., Armstrong, R. T., Jansik, D. P., Wood, B. D., & Wildenschild, D. (2011). Imaging biofilm architecture within porous media using synchrotron-based X-ray computed microtomography. *Water Resources Research*, *47*(2). https://doi.org/10.1029/2010wr009410
Jaisi, D. P., Saleh, N. B., Blake, R. E., & Elimelech, M. (2008). Transport of single-walled carbon nanotubes in porous media: Filtration mechanisms and reversibility. *Environmental Science & Technology*, *42*(22), 8317–8323. https://doi.org/10.1021/es801641v
Johnson, P. R., Sun, N., & Elimelech, M. (1996). Colloid transport in geochemically heterogeneous porous media: Modeling and measurements. *Environmental Science & Technology*, *30*(11), 3284–3293. https://doi.org/10.1021/es960053+
Johnson, W. P., Li, X., & Yal, G. (2007). Colloid retention in porous media: Mechanistic confirmation of wedging and retention in zones of flow stagnation. *Environmental Science & Technology*, *41*(4), 1279–1287. https://doi.org/10.1021/es061301x
Johnson, W. P., Pazmino, E., & Ma, H. (2010). Direct observations of colloid retention in granular media in the presence of energy barriers, and implications for inferred mechanisms from indirect observations. *Water Research*, *44*(4), 1158–1169. https://doi.org/10.1016/j.watres.2009.12.014
Johnson, W. P., Rasmuson, A., Pazmiño, E., & Hilpert, M. (2018). Why variant colloid transport behaviors emerge among identical individuals in porous media when colloid–surface repulsion exists. *Environmental Science & Technology*, *52*(13), 7230–7239. https://doi.org/10.1021/acs.est.8b00811

Kaegi, R., Voegelin, A., Sinnet, B., Zuleeg, S., Hagendorfer, H., Burkhardt, M., & Siegrist, H. (2011). Behavior of metallic silver nanoparticles in a pilot wastewater treatment plant. *Environmrntal Science & Technology*, *45*(9), 3902–3908. https://doi.org/10.1021/es1041892

Keller, A. A., Vosti, W., Wang, H., & Lazareva, A. (2014). Release of engineered nanomaterials from personal care products throughout their life cycle. *Journal of Nanoparticle Research*, *16*(7), 2489. https://doi.org/10.1007/s11051-014-2489-9

Ko, C.-H., & Elimelech, M. (2000). The "shadow effect" in colloid transport and deposition dynamics in granular porous media: Measurements and mechanisms. *Environmental Science & Technology*, *34*(17), 3681–3689. https://doi.org/10.1021/es0009323

Kohli, R., & Mittal, K. L. (2015). Developments in surface contamination and cleaning. In *Fundamentals and Applied Aspects* (Vol. 1). William Andrew.

Kuempel, E. D., Roberts, J. R., Roth, G., Zumwalde, R. D., Nathan, D., Hubbs, A. F., et al. (2021). *Current intelligence bulletin 70: Health effects of occupational exposure to silver nanomaterials*. U.S. Department of Health and Human Services, Centers for Disease Control and Prevention, National Institute for Occupational Safety and Health, DHHS (NIOSH).

Lazouskaya, V., Jin, Y., & Or, D. (2006). Interfacial interactions and colloid retention under steady flows in a capillary channel (vol 303, pg 171, 2006). *Journal of Colloid and Interface Science*, *405*, 346. https://doi.org/10.1016/j.jcis.2013.05.001

Leuther, F., Köhne, J. M., Metreveli, G., & Vogel, H.-J. (2020). Transport and retention of sulfidized silver nanoparticles in porous media: The role of air-water interfaces, flow velocity, and natural organic matter. *Water Resources Research*, *56*(9), e2020WR027074. https://doi.org/10.1029/2020wr027074

Li, X., Lin, C.-L., Miller, J. D., & Johnson, W. P. (2006a). Pore-scale observation of microsphere deposition at grain-to-grain contacts over assemblage-scale porous media domains using X-ray microtomography. *Environmental Science & Technology*, *40*(12), 3762–3768. https://doi.org/10.1021/es0525004

Li, X., Lin, C.-L., Miller, J. D., & Johnson, W. P. (2006b). Role of grain-to-grain contacts on profiles of retained colloids in porous media in the presence of an energy barrier to deposition. *Environmental Science & Technology*, *40*(12), 3769–3774. https://doi.org/10.1021/es052501w

Lin, D., Hu, L., Bradford, S. A., Zhang, X., & Lo, I. (2021). Simulation of colloid transport and retention using a pore-network model with roughness and chemical heterogeneity on pore surfaces. *Water Resources Research*, *57*(2), e2020WR028571. https://doi.org/10.1029/2020wr028571

Lin, S., & Wiesner, M. R. (2012). Paradox of stability of nanoparticles at very low ionic strength. *Langmuir*, *28*(30), 11032–11041. https://doi.org/10.1021/la3016589

Maillard, J.-Y., & Hartemann, P. (2013). Silver as an antimicrobial: Facts and gaps in knowledge. *Critial Reviews Microbiology*, *39*(4), 373–383. https://doi.org/10.3109/1040841x.2012.713323

Malgaresi, G., Collins, B., Alvaro, P., & Bedrikovetsky, P. (2019). Explaining non-monotonic retention profiles during flow of size-distributed colloids. *Chemical Engineering Journal*, *375*, 121984. https://doi.org/10.1016/j.cej.2019.121984

Marley, N. A., Gaffney, J. S., Orlandini, K. A., & Cunningham, M. M. (1993). Evidence for radionuclide transport and mobilization in a shallow, sandy aquifer. *Environmental Science & Technology*, *27*(12), 2456–2461. https://doi.org/10.1021/es00048a022

Mibus, J., Sachs, S., Pfingsten, W., Nebelung, C., & Bernhard, G. (2007). Migration of uranium (IV)/(VI) in the presence of humic acids in quartz sand: A laboratory column study. *Journal of Contaminant Hydrology*, *89*(3–4), 199–217. https://doi.org/10.1016/j.jconhyd.2006.08.005

Mijnendonckx, K., Leys, N., Mahillon, J., Silver, S., & Van Houdt, R. (2013). Antimicrobial silver: Uses, toxicity and potential for resistance. *Biometals*, *26*(4), 609–621. https://doi.org/10.1007/s10534-013-9645-z

Mills, A. L., Herman, J. S., Hornberger, G. M., & DeJesús, T. H. (1994). Effect of solution ionic strength and iron coatings on mineral grains on the sorption of bacterial cells to quartz sand. *Applied and Environmental Microbiology*, *60*(9), 3300–3306. https://doi.org/10.1128/aem.60.9.3300-3306.1994

Molnar, I., Gerhard, J. I., Willson, C. S., & O'Carroll, D. M. (2015). The impact of immobile zones on the transport and retention of nanoparticles in porous media. *Water Resources Research*, *51*(11), 8973–8994. https://doi.org/10.1002/2015wr017167

Molnar, I., Johnson, W. P., Gerhard, J. I., Willson, C. S., & O'Carroll, D. M. (2015). Predicting colloid transport through saturated porous media: A critical review. *Water Resources Research*, *51*(9), 6804–6845. https://doi.org/10.1002/2015wr017318

Morales, V. L., Dentz, M., Willmann, M., & Holzner, M. (2017). Stochastic dynamics of intermittent pore-scale particle motion in three-dimensional porous media: Experiments and theory. *Geophysical Research Letters*, *44*(18), 9361–9371. https://doi.org/10.1002/2017gl074326

Morales, V. L., Gao, B., & Steenhuis, T. S. (2009). Grain surface-roughness effects on colloidal retention in the vadose zone. *Vadose Zone Journal*, *8*(1), 11–20. https://doi.org/10.2136/vzj2007.0171

Morales, V. L., Sang, W., Fuka, D. R., Lion, L. W., Gao, B., & Steenhuis, T. S. (2011). Correlation equation for predicting attachment efficiency (α) of organic matter-colloid complexes in unsaturated porous media. *Environmental Science & Technology*, *45*(23), 10096–10101. https://doi.org/10.1021/es2023829

Morales, V. L., Zhang, W., Gao, B., Lion, L. W., Bisogni, J. J., Jr., McDonough, B. A., & Steenhuis, T. S. (2011). Impact of dissolved organic matter on colloid transport in the vadose zone: Deterministic approximation of transport deposition coefficients from polymeric coating characteristics. *Water Research*, *45*(4), 1691–1701. https://doi.org/10.1016/j.watres.2010.10.030

Park, E.-J., Bae, E., Yi, J., Kim, Y., Choi, K., Lee, S. H., et al. (2010). Repeated-dose toxicity and inflammatory responses in mice by oral administration of silver nanoparticles. *Environmental Toxicology and Pharmacology*, *30*(2), 162–168. https://doi.org/10.1016/j.etap.2010.05.004

Patiño, J. E., Kuhl, T. L., & Morales, V. L. (2020). Direct measurements of the forces between silver and mica in humic substance-rich solutions. *Environmental Science & Technology*, *54*(23), 15076–15085. https://doi.org/10.1021/acs.est.0c05334

Perez, A. J., Patino, J. E., Soos, M., & Morales, V. L. (2020). Morphology of shear-induced colloidal aggregates in porous media: Consequences for transport, deposition, and re-entrainment. *Environmental Science & Technology*, *54*(9), 5813–5821. https://doi.org/10.1021/acs.est.9b05744

Phenrat, T., Saleh, N., Sirk, K., Kim, H.-J., Tilton, R. D., & Lowry, G. V. (2008). Stabilization of aqueous nanoscale zerovalent iron dispersions by anionic polyelectrolytes: Adsorbed anionic polyelectrolyte layer properties and their effect on aggregation and sedimentation. *Journal of Nanoparticle Research*, *10*(5), 795–814. https://doi.org/10.1007/s11051-007-9315-6

Polemio, M., Bufo, S., & Paoletti, S. (1980). Evaluation of ionic strength and salinity of groundwaters: Effect of the ionic composition. *Geochimica et Cosmochimica Acta*, *44*(6), 809–814. https://doi.org/10.1016/0016-7037(80)90262-8

Rahmatpour, S., Mosaddeghi, M. R., Shirvani, M., & Simunek, J. (2018). Transport of silver nanoparticles in intact columns of calcareous soils: The role of flow conditions and soil texture. *Geoderma*, *322*, 89–100. https://doi.org/10.1016/j.geoderma.2018.02.016

Rasmuson, A., Pazmino, E., Assemi, S., & Johnson, W. P. (2017). Contribution of nano-to microscale roughness to heterogeneity: Closing the gap between unfavorable and favorable colloid attachment conditions. *Environmental Science & Technology*, *51*(4), 2151–2160. https://doi.org/10.1021/acs.est.6b05911

Ron, C. A., & Johnson, W. P. (2020). Complementary colloid and collector nanoscale heterogeneity explains microparticle retention under unfavorable conditions. *Environmental Sciences: Nano*, *7*(12), 4010–4021. https://doi.org/10.1039/d0en00815j

Samarajeewa, A., Velicogna, J., Princz, J., Subasinghe, R., Scroggins, R., & Beaudette, L. (2017). Effect of silver nano-particles on soil microbial growth, activity and community diversity in a sandy loam soil. *Environmental Pollution*, *220*, 504–513. https://doi.org/10.1016/j.envpol.2016.09.094

Sen, T. K., & Khilar, K. C. (2006). Review on subsurface colloids and colloid-associated contaminant transport in saturated porous media. *Advances in Colloid and Interface Science*, *119*(2–3), 71–96. https://doi.org/10.1016/j.cis.2005.09.001

Shen, C., Li, B., Huang, Y., & Jin, Y. (2007). Kinetics of coupled primary-and secondary-minimum deposition of colloids under unfavorable chemical conditions. *Environmental Science & Technology*, *41*(20), 6976–6982. https://doi.org/10.1021/es070210c

Sillen, W. M., Thijs, S., Abbamondi, G. R., Janssen, J., Weyens, N., White, J. C., & Vangronsveld, J. (2015). Effects of silver nanoparticles on soil microorganisms and maize biomass are linked in the rhizosphere. *Soil Biology and Biochemistry*, *91*, 14–22. https://doi.org/10.1016/j.soilbio.2015.08.019

Sirivithayapakorn, S., & Keller, A. (2003). Transport of colloids in unsaturated porous media: A pore-scale observation of processes during the dissolution of air-water interface. *Water Resources Research*, *39*(12). https://doi.org/10.1029/2003wr002487

Smulders, E., & Rähse, W. (2002). *Laundry detergents*. Wiley Online Library.

Sondi, I., & Salopek-Sondi, B. (2004). Silver nanoparticles as antimicrobial agent: A case study on E. coli as a model for Gram-negative bacteria. *Journal of Colloid and Interface Science*, *275*(1), 177–182. https://doi.org/10.1016/j.jcis.2004.02.012

Torkzaban, S., & Bradford, S. A. (2016). Critical role of surface roughness on colloid retention and release in porous media. *Water Research*, *88*, 274–284. https://doi.org/10.1016/j.watres.2015.10.022

Torkzaban, S., Bradford, S. A., & Walker, S. L. (2007). Resolving the coupled effects of hydrodynamics and DLVO forces on colloid attachment in porous media. *Langmuir*, *23*(19), 9652–9660. https://doi.org/10.1021/la700995e

Torkzaban, S., Tazehkand, S. S., Walker, S. L., & Bradford, S. A. (2008). Transport and fate of bacteria in porous media: Coupled effects of chemical conditions and pore space geometry. *Water Resources Research*, *44*(4). https://doi.org/10.1029/2007wr006541

Tosco, T., Papini, M. P., Viggi, C. C., & Sethi, R. (2014). Nanoscale zerovalent iron particles for groundwater remediation: A review. *Journal of Cleaner Production*, *77*, 10–21. https://doi.org/10.1016/j.jclepro.2013.12.026

Tufenkji, N., & Elimelech, M. (2004). Deviation from the classical colloid filtration theory in the presence of repulsive DLVO interactions. *Langmuir*, *20*(25), 10818–10828. https://doi.org/10.1021/la0486638

Tufenkji, N., & Elimelech, M. (2005). Breakdown of colloid filtration theory: Role of the secondary energy minimum and surface charge heterogeneities. *Langmuir*, *21*(3), 841–852. https://doi.org/10.1021/la048102g

Tulve, N. S., Stefaniak, A. B., Vance, M. E., Rogers, K., Mwilu, S., LeBouf, R. F., et al. (2015). Characterization of silver nanoparticles in selected consumer products and its relevance for predicting children's potential exposures. *International Journal of Hygiene and Environmental Health*, *218*(3), 345–357. https://doi.org/10.1016/j.ijheh.2015.02.002

Van Oss, C. J. (2006). *Interfacial forces in aqueous media*. CRC press.

Verwey, E., & Willem, J. (1947). Theory of the stability of lyophobic colloids. *The Journal of Physical Chemistry*, *51*(3), 631–636. https://doi.org/10.1021/j150453a001

Wan, J., & Tokunaga, T. K. (1997). Film straining of colloids in unsaturated porous media: Conceptual model and experimental testing. *Environmental Science & Technology*, *31*(8), 2413–2420. https://doi.org/10.1021/es970017q

Wan, J., & Tokunaga, T. K. (2005). Comments on "pore-scale visualization of colloid transport and retention in partly saturated porous media". *Vadose Zone Journal*, *4*(4), 954–956. https://doi.org/10.2136/vzj2005.0010

Wan, J., & Wilson, J. L. (1994). Colloid transport in unsaturated porous media. *Water Resources Research*, *30*(4), 857–864. https://doi.org/10.1029/93wr03017

Wielinski, J., Gogos, A., Voegelin, A., Müller, C. R., Morgenroth, E., & Kaegi, R. (2021). Release of gold (Au), silver (Ag) and cerium dioxide (CeO 2) nanoparticles from sewage sludge incineration ash. *Environmental Sciences: Nano*, *8*(11), 3220–3232. https://doi.org/10.1039/d1en00497b

Wood, J. A., & Rehmann, L. (2014). Geometric effects on non-DLVO forces: Relevance for nanosystems. *Langmuir*, *30*(16), 4623–4632. https://doi.org/10.1021/la500664c

Yao, K.-M., Habibian, M. T., & O'Melia, C. R. (1971). Water and waste water filtration. concepts and applications. *Environmental Science & Technology*, *5*(11), 1105–1112. https://doi.org/10.1021/es60058a005

Yoon, R.-H., & Mao, L. (1996). Application of extended DLVO theory, IV: Derivation of flotation rate equation from first principles. *Journal of Colloid and Interface Science*, *181*(2), 613–626. https://doi.org/10.1006/jcis.1996.0419

Zevi, Y., Gao, B., Zhang, W., Morales, V. L., Cakmak, M. E., Medrano, E. A., et al. (2012). Colloid retention at the meniscus-wall contact line in an open microchannel. *Water Research*, *46*(2), 295–306. https://doi.org/10.1016/j.watres.2011.09.046

Zhang, C., Hu, Z., & Deng, B. (2016). Silver nanoparticles in aquatic environments: Physiochemical behavior and antimicrobial mechanisms. *Water Research*, *88*, 403–427. https://doi.org/10.1016/j.watres.2015.10.025

Zhang, H., Huang, M., Zhang, W., Gardea-Torresdey, J. L., White, J. C., Ji, R., & Zhao, L. (2020). Silver nanoparticles alter soil microbial community compositions and metabolite profiles in unplanted and cucumber-planted soils. *Environmental Science & Technology*, *54*(6), 3334–3342. https://doi.org/10.1021/acs.est.9b07562

References From the Supporting Information

Bartell, F., & Smith, J. (1953). Alteration of surface properties of gold and silver as indicated by contact angle measurements. *The Journal of Physical Chemistry*, *57* (2), 165–172.

Gadre, K. S., & Alford, T. (2003). Contact angle measurements for adhesion energy evaluation of silver and copper films on parylene-n and SiO_2 substrates. *Journal of applied physics*, *93* (2), 919–923.

Yoon, R.-H., & Aksoy, B. S. (1999). Hydrophobic forces in thin water films stabilized by dodecylammonium chloride. *Journal of Colloid and Interface Science*, *211* (1), 1–10.

Yoon, R.-H., & Mao, L. (1996). Application of extended DLVO theory, IV: Derivation of flotation rate equation from first principles. *Journal of Colloid and Interface Science*.